Applied Catalysis B: Environmental 130–131 (2013) 93–98

Contents lists available at SciVerse ScienceDirect

Applied Catalysis B: Environmental

journal homepage: www.elsevier.com/locate/apcatb

Interfacial charge carrier dynamics of type-II semiconductor nanoheterostructures

Yi-Fang Lin, Yung-Jung Hsu*

Department of Materials Science and Engineering, National Chiao Tung University, 1001 University Road, Hsinchu 30010, Taiwan, ROC

ARTICLE INFO

Article history:
Received 15 August 2012
Received in revised form 19 October 2012
Accepted 28 October 2012
Available online 7 November 2012

Keywords:
Type-II semiconductor nanoheterostructures
Charge separation
Photoconversion
Photocatalysis
CdS nanowires

ABSTRACT

Semiconductor nanoheterostructures with type-II band offset have exhibited unique optoelectronic properties that are beneficial to photoconversion applications. Debatable arguments however exist in the literature for interpreting the most enhanced photocatalytic performance of type-II semiconductor nanoheterostructures when an optimal content of the constituents is employed. In this work, time-resolved photoluminescence is used to investigate the interfacial charge carrier dynamics for $CdSnO_3$-decorated CdS nanowires, a prototype type-II nanoheterostructures system, with varying $CdSnO_3$ contents. Our results show that the $CdSnO_3$ content of 2.5 at% rendered CdS–$CdSnO_3$ NWs the most significant charge carrier separation, above which electron–hole recombination across CdS/$CdSnO_3$ interface mediated carrier transfer to compromise the overall charge separation efficiency. The carrier dynamics results are in good accordance with that of photoconversion performance evaluation in dye photodegradation, which assists in resolving the very critical but still controversial issue as to the factors causing the depressed photocatalytic efficiency of type-II nanoheterostructures when the constituent content exceeds the optimal value.

1. Introduction

With the inherently high degree of complexity, nanoheterostructures composed of two or more materials joined in unique architectures may exhibit superior synergetic properties that are difficult or impossible to acquire from their individual constituents. Of particular interest are the type-II semiconductor nanoheterostructures, where the relative band alignment of the constituents promotes effective charge separation to bring them desirable properties for photoconversion applications [1–14]. For example, with the decoration of Ag_2O nanoparticles, TiO_2 nanobelts displayed significantly enhanced photocatalytic activities under both ultraviolet and visible light illumination. This enhancement results from the staggered band offset between Ag_2O and TiO_2, which inhibits charge recombination to capture more charge carriers for participation in photocatalysis [8]. Besides, a five-fold increase in photoconversion efficiency was observed for TiO_2 nanotubes once they were coated with a thin layer of CdS. This improvement is due to the more negative conduction band of CdS, which ensures a quick electron transfer from CdS to TiO_2 and thus the facilitated collection of electrons [10]. Till now, various kinds of semiconductor nanoheterostructures with type-II band offset have been proposed and fabricated to further the advancement of photoconversion technology.

To comprehend the factors dictating the photoconversion efficiency of type-II semiconductor nanoheterostructures, several research groups have focused on realizing the interfacial charge carrier dynamics using ultrafast laser spectroscopy techniques [15–20]. Primary results show that the difference in conduction band energy level between the two constituents of type-II nanoheterostructures determines the driving force for interfacial charge transfer and thereby governs the charge separation property. By enlarging this energy difference, type-II nanoheterostructures may exhibit significantly improved charge separation and performed better in photoconversion applications [18–20]. Besides the energy difference, the relative content of the constituents of nanoheterostructures affects the resultant photoconversion efficiency as well. It has been extensively observed that there exists an optimal content of each constituent for enhancing the photocatalytic efficiency of type-II semiconductor nanoheterostructures [21–30]. This phenomenon has often been ambiguously ascribed to issues like inhibited light absorption [21–24], structural effect [21,25,26], charge trapping [27,28], or even no apparent reasons [29,30]. Moreover, there are very few studies in the literature regarding the dependence of interfacial charge transfer on the relative content of the constituents for such nanoheterostructures, and their correlation with the resultant photoconversion efficiency has never been reported. Therefore, a quantitative study on this subject is crucial to both the fundamental

* Corresponding author. Tel.: +886 3 5712121x55317; fax: +886 3 5724724.
E-mail addresses: yhsu@cc.nctu.edu.tw, yhsu@mail.nctu.edu.tw (Y.-J. Hsu).

0926-3373/$ – see front matter © 2012 Elsevier B.V. All rights reserved.
http://dx.doi.org/10.1016/j.apcatb.2012.10.024

Table 1
Kinetic analysis of emission decay for pristine CdS and different CdS–$CdSnO_3$ NWs.

	$A_1/(A_1+A_2)$ (%)	τ_1 (ns)	$A_2/(A_1+A_2)$ (%)	τ_2 (ns)	k_{et} (s^{-1})
Pristine CdS	26.4	8.03	73.6	2.19	–
CdS–$CdSnO_3$, 1.25 at%	22.0	5.22	78.0	0.57	1.30×10^9
CdS–$CdSnO_3$, 2.5 at%	5.6	4.69	94.4	0.24	3.71×10^9
CdS–$CdSnO_3$, 5.0 at%	11.6	4.84	88.4	0.30	2.88×10^9
CdS–$CdSnO_3$, 10.0 at%	30.1	6.48	69.9	1.36	0.28×10^9

understanding and the practical applications for type-II semiconductor nanoheterostructures.

In this work, we presented a prototype type-II semiconductor nanoheterostructures system by combining CdS and $CdSnO_3$ into a single hybrid. The samples were prepared by depositing $CdSnO_3$ nanocrystals on the surface of CdS nanowires (denoted as CdS–$CdSnO_3$ NWs) in the solvothermal reaction. For CdS–$CdSnO_3$ NWs, the surface-attached $CdSnO_3$ can serve as an effective electron scavenger for CdS due to its lower conduction band potential (+0.9 V vs. NHE) than that of CdS (−0.5 V vs. NHE) [31,32]. Consequently, the photoexcited electrons of CdS NWs would preferentially transfer to $CdSnO_3$ nanocrystals, leaving photogenerated holes at CdS domain to achieve charge carrier separation. Time-resolved photoluminescence (PL) measurements were conducted to explore the interfacial charge carrier dynamics for the as-prepared CdS–$CdSnO_3$ NWs. By probing the emission lifetime of CdS, the electron transfer event between CdS and $CdSnO_3$ for CdS–$CdSnO_3$ NWs and its dependence on $CdSnO_3$ content were quantitatively analyzed. A $CdSnO_3$ content of 2.5 at% was found to render CdS–$CdSnO_3$ NWs the most significant charge carrier separation, above which electron–hole recombination across interface mediated carrier transfer to compromise the overall charge separation efficiency. This consequence is in good agreement with the result of photoconversion performance evaluation in dye photodegradation, which helps to resolve debatable arguments about the factors causing the depressed photocatalytic efficiency of type-II semiconductor nanoheterostructures when the constituent content exceeds the optimal value.

2. Experimental

2.1. Chemicals

All chemicals were analytic-grade and used without further purification. Special attention should be paid when dealing with the hazardous Cd source.

2.2. NWs syntheses

The syntheses of pristine CdS and CdS–$CdSnO_3$ NWs were conducted in a solvothermal process [33]. For the preparation of CdS NWs, $Cd(NO_3)_2 \cdot 4H_2O$ (1.54 g, 0.005 mol) and sulfur powder (0.32 g, 0.01 mol) were mixed with ethylenediamine (80 mL) in the flask. The solution was then transferred to a Teflon-lined stainless steel autoclave (with a capacity of 100 mL) for solvothermal reaction at 180 °C for 24 h. The resulting yellow solid product (CdS NWs) was centrifuged, and washed with distilled water and ethanol to remove remaining ions. With the addition of $SnCl_2 \cdot 2H_2O$ (11.28 mg, 0.05 mmol) and NaOH (0.02 mL, 5 M) in the solvothermal reaction, growth of CdS NWs was accompanied by the deposition of $CdSnO_3$ nanocrystals, resulting in the formation of CdS–$CdSnO_3$ NWs. In this work, various concentrations of $SnCl_2 \cdot 2H_2O$ (0.00625, 0.0125, 0.025, 0.05 mmol) added in the reaction solution were employed to produce CdS–$CdSnO_3$ NWs with different $CdSnO_3$ contents (1.25, 2.5, 5.0, 10.0 at%, respectively). For comparison purpose, pure $CdSnO_3$ nanocrystals were also prepared.

2.3. PL lifetime measurement

Time-resolved PL spectra were measured using a home-built single photon counting system (Horiba Jobin Yvon) which delivers an instrument response function down to 25 ps FWHM. GaN diode laser (λ = 375 nm) was used as the excitation source. The signals collected at the excitonic emission of CdS (λ_{em} = 502 nm) were dispersed with a grating spectrometer, detected by a high-speed photomultiplier tube, and then correlated using a single photon counting card. Upon laser excitation, the photoexcited electrons of CdS were injected into $CdSnO_3$ due to the higher conduction band potential of CdS (−0.5 V vs. NHE) than that of $CdSnO_3$ (+0.9 V vs. NHE), which leads to a significant quenching on the emission of CdS. By comparing the emission decay profiles between CdS and CdS–$CdSnO_3$, the electron transfer from CdS to $CdSnO_3$ can be quantitatively deduced. It should be noted that $CdSnO_3$ did not exhibited PL emission around 500 nm, with which the emission decay of CdS at 502 nm was not interfered and its variation with the presence of $CdSnO_3$ can be precisely interpreted. The emission decay data were analyzed and fitted with biexponential kinetics model which generates two lifetime values, τ_1 and τ_2, and the corresponding amplitudes, A_1 and A_2. All the fitting results were summarized in Table 1. The value of goodness (χ^2) of the fitting was in the range of 1.00–1.06, indicating a good fit to the experimental data.

2.4. Photodegradation experiment

The photodegradation experiment on CdS–$CdSnO_3$ NWs was carried out by using rhodamine B (RhB) as the probe molecule under visible light illumination. A quartz tube with a capacity of 30 mL was used as the photoreactor vessel. The optical system used for photodegradation consisted of a xenon lamp (500 W, with a light intensity of 175 mW/cm^2) and a bandpass filter (with the bandwidth of 400–700 nm) that allowed the irradiation in visible range. Six kinds of samples including pristine CdS NWs, four CdS–$CdSnO_3$ NWs, and pure $CdSnO_3$ nanocrystals were compared in the photodegradation of RhB. Typically, a fixed amount of sample (3 mg) was added into RhB aqueous solution (15 mL, 1.0×10^{-5} M) in the photoreactor vessel. Prior to irradiation, the suspension was aerated and stirred in the dark for 30 min to reach the adsorption equilibrium between RhB and sample. Dye adsorption capability of the sample was then evaluated by measuring the RhB concentration change after the adsorption equilibrium. At certain time intervals of irradiation, 1.5 mL of the reaction solution was withdrawn and centrifuged to remove sample particles. The filtrates were analyzed with a UV–visible spectrophotometer to measure the concentration variation of RhB through recording the corresponding absorbance of the characteristic peak at 554 nm. Furthermore, photodegradation of RhB (1.0×10^{-5} M) under natural sunlight by using CdS–$CdSnO_3$ NWs (3 mg) was also tested.

2.5. Characterizations

The morphology and dimensions of the samples were examined with a field-emission scanning electron microscope (SEM, JEOL, JSM-6500F) and a high-resolution transmission electron

microscope (HRTEM, JEOL, JEM-3000) operated at 300 kV. The crystallographic structure of the samples was investigated with X-ray diffraction (XRD, MAC Science, MXP18). The elemental analysis of NWs was conducted with the energy dispersive X-ray spectrometry (EDS), the accessory of SEM (JSM-6500F) and TEM (JEM-3000). For steady-state PL spectroscopy, a Kimmon IK3001R-G equipped with He-Cd laser (720 W) was used. UV–visible absorption spectra were obtained using a Hitachi U-3900H spectrophotometer at room temperature.

3. Results and discussion

Single-crystalline CdS NWs with the diameter of 30–50 nm were obtained from a typical solvothermal process. With the addition of $SnCl_2$ and NaOH in the solvothermal reaction, growth of CdS NWs was accompanied by the decoration of cube-shaped nanocrystals. As shown in Fig. 1, the surface-attached nanocrystals had the size of 100–120 nm and also possessed single crystallinity. The composition of these nanocrystals was confirmed as $CdSnO_3$ from the corresponding TEM-EDS and XRD analyses. In Fig. 1(c), the HRTEM image clearly reveals the substantial interface of CdS/$CdSnO_3$ that formed in CdS–$CdSnO_3$ NWs. This interface was considerably important since it ensured the successful electron transfer from CdS to $CdSnO_3$ upon light irradiation and thus the achievement of charge separation. Fig. 2 represents the structural investigation of CdS–$CdSnO_3$ NWs prepared with different $SnCl_2$ concentrations. Evidently, as increasing the concentration of $SnCl_2$ added, the amount of $CdSnO_3$ nanocrystals deposited on CdS NWs increased accordingly. From SEM-EDS analysis, the content of $CdSnO_3$ deposited on CdS NWs was relatively determined to be 1.25, 2.5, 5.0, and 10.0 at%. With this outcome, we were able to study the quantitative effect of $CdSnO_3$ decoration on the charge carrier dynamics of CdS NWs. Besides, it is important to note that free-standing $CdSnO_3$ nanocrystals were rarely observed in the products, demonstrating the accuracy of the $CdSnO_3$ content determined and the validity of the quantitative effect of CdSnO3 decoration.

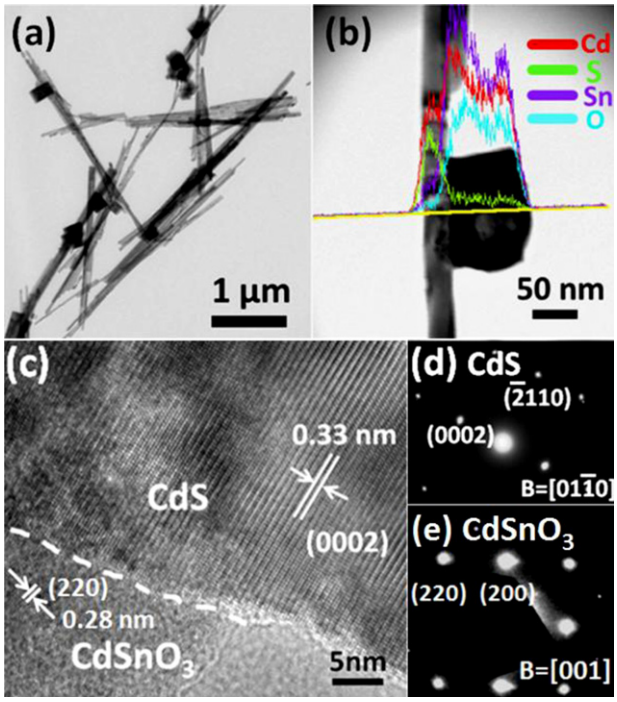

Fig. 1. (a) TEM image, (b) TEM-EDS analysis, and (c) HRTEM image of CdS–$CdSnO_3$ NWs. In (c), the CdS/$CdSnO_3$ interface was highlighted by a dashed line. The electron diffraction pattern respectively taken at NW and nanocrystal region was shown in (d) and (e).

The present CdS–$CdSnO_3$ NWs provided an ideal platform to investigate the interfacial charge transfer property of type-II semiconductor nanoheterostructures. Owing to the difference in band

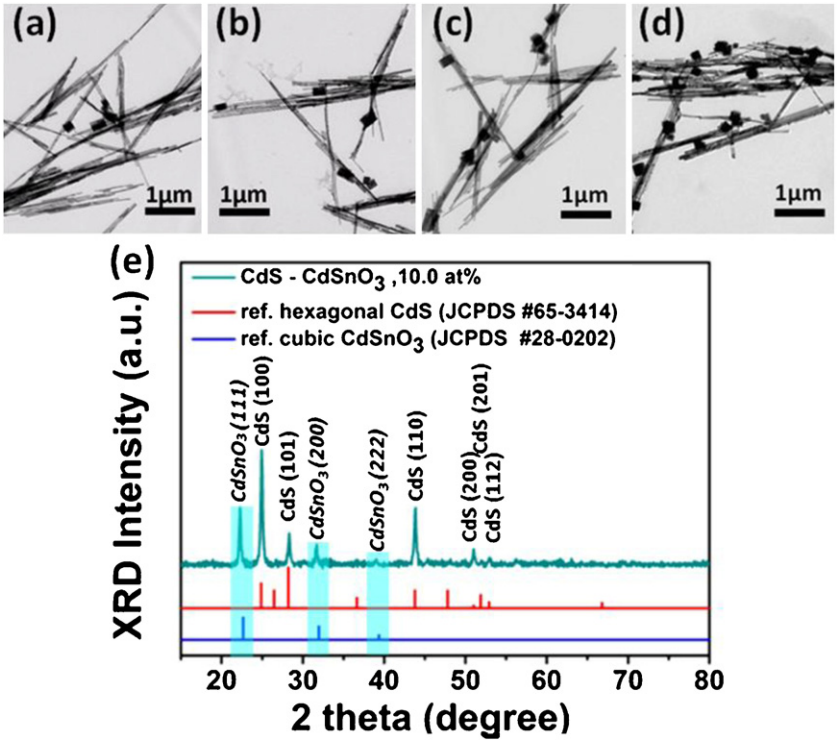

Fig. 2. TEM images of CdS–$CdSnO_3$ NWs with $CdSnO_3$ content of (a) 1.25, (b) 2.5, (c) 5.0, and (d) 10.0 at%. The corresponding XRD pattern was shown in (e), and the diffraction peaks from $CdSnO_3$ were highlighted by colored bars.

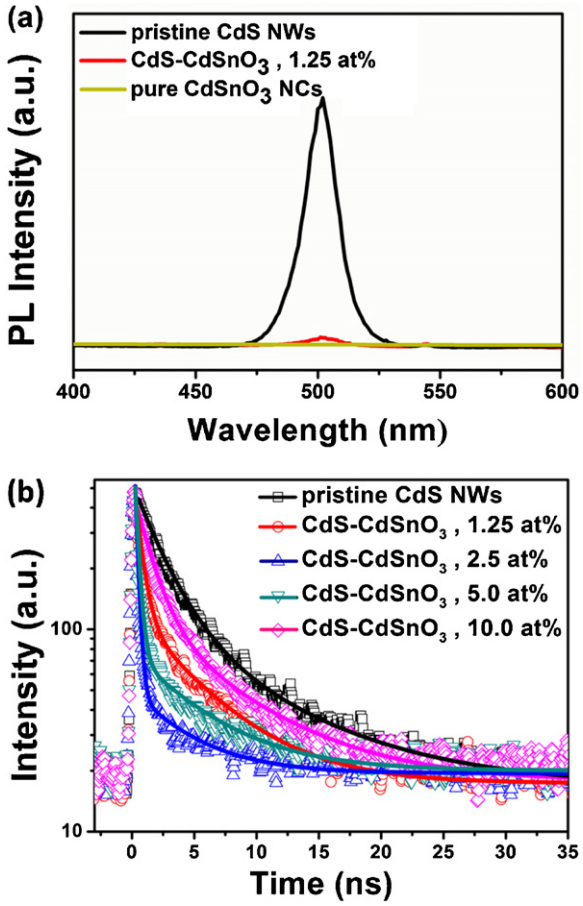

Fig. 3. (a) Steady-state PL and (b) time-resolved PL spectra for pristine CdS and CdS–$CdSnO_3$ NWs with different $CdSnO_3$ contents. In (b), the fitting results (solid curves) were also included for comparison.

structure between CdS and $CdSnO_3$, most of the photoexcited electrons of CdS NWs would transfer to $CdSnO_3$ nanocrystals, leading to the depletion of free electrons for CdS and the subsequent suppression of its excitonic emission. Fig. 3(a) compares the steady-state PL spectra of pristine CdS and CdS–$CdSnO_3$ NWs. The pristine CdS NWs exhibited a prominent emission at 502 nm, attributable to the typical excitonic band-to-band radiative emission of CdS [34]. As to CdS–$CdSnO_3$ NWs, a significant depression in PL emission was recorded. Since there was no spectral overlap between PL of CdS and absorption of $CdSnO_3$ (E_g = 3.1 eV, absorption onset was around 400 nm), the contribution of energy transfer to the as-observed PL depression for CdS–$CdSnO_3$ can be excluded [35,36]. This manifests that electron transfer from CdS to $CdSnO_3$ dominated the emission quenching of CdS–$CdSnO_3$ NWs. If the observed PL depression of CdS–$CdSnO_3$ NWs indeed arose from the electron transfer from CdS to $CdSnO_3$, we should be able to reveal this event in the emission decay profile of CdS. Fig. 3(b) represents the time-resolved PL spectra of pristine CdS and the four CdS–$CdSnO_3$ NWs. Consistent with steady-state PL quenching, introduction of $CdSnO_3$ nanocrystals reduced the emission lifetime of CdS NWs. These spectra were fitted with a biexponential function which yields a slow (τ_1) and a fast (τ_2) decay component relatively assigned to radiative recombination and nonradiative relaxation pathway [37,38]. The fitting results were summarized in Table 1. For pristine CdS, 73.6% of excited states were deactivated with a 2.19 ns lifetime (τ_2), which was followed by a 26.4% slow decay of 8.03 ns (τ_1). Upon the introduction of 1.25 at% $CdSnO_3$, the fast decay component of CdS was highly reduced to 0.57 ns with a slightly enhanced amplitude contribution of 78.0%. This result indicates the emergence of additional nonradiative pathway from the electronic interaction between CdS and $CdSnO_3$, which can be verified by the steady-state PL depression observed for CdS–$CdSnO_3$ NWs. Assuming electron transfer from CdS to $CdSnO_3$ was the predominant process dictating the emission quenching of CdS for CdS–$CdSnO_3$, we can estimate the electron-transfer rate constant (k_{et}) from the emission lifetime data by the expression k_{et} (CdS → $CdSnO_3$) = $(1/\tau_2)$(CdS–$CdSnO_3$) − $(1/\tau_2)$(CdS) [39], approximately 1.30×10^9 s^{-1} for CdS–$CdSnO_3$ NWs with $CdSnO_3$ content of 1.25 at%. By comparing the rate constants of CdS and CdS–$CdSnO_3$ NWs [40,41], we calculated that 74.0% of the electrons generated at CdS following photoexcitation were transferred across the CdS/$CdSnO_3$ interface. It should be noted that although electron trapping at the CdS/$CdSnO_3$ interface might occur to conduce to the variation in emission decay profile, we supposed this contribution was relatively minor based on the considerably low content of $CdSnO_3$ and the significant enhancement in the resultant photoconversion efficiency, as will be demonstrated later.

Similar to the system of In_2O_3–TiO_2–Pt where the electron transfer from TiO_2 to Pt was dependent on Pt concentration [17], $CdSnO_3$ in the present CdS–$CdSnO_3$ NWs also had a quantitative effect. As noted in Table 1, when $CdSnO_3$ content was increased from 1.25 to 2.5 at%, the fast decay component of CdS was shortened from 0.57 to 0.24 ns. This phenomenon signifies that $CdSnO_3$ of 2.5 at% affected the charge carrier dynamics of CdS more significantly by attracting more photoexcited electrons from CdS, which leads to the more pronounced charge carrier separation for CdS–$CdSnO_3$ NWs with the k_{et} of 3.71×10^9 s^{-1}. The significantly enhanced amplitude contribution from the fast decay component (94.4%) and its dominance over the slow decay term (5.6%) supported the above proposition. Further increase in the content of $CdSnO_3$ (5.0 at%) however caused a lengthened time constant for the fast decay component of CdS (τ_2 = 0.30 ns), suggesting that electron scavenging from CdS as well as charge carrier separation turned decreasingly conspicuous as $CdSnO_3$ of 5.0 at% was introduced. The corresponding k_{et} was estimated to be 2.88×10^9 s^{-1}. Note that when electron scavenger with an excess amount was present, the overall charge separation efficiency of semiconductor nanoheterostructures would decline [42–45]. This detrimental effect derives from the consumption of the separated electrons in the later-emerging electron–hole recombination process, which alleviated the extent of electron scavenging to result in the less effective charge carrier separation [17]. At relatively high $CdSnO_3$ content of 5.0 at%, electrons trapped at $CdSnO_3$ were such abundant that recombination of charge carriers across the CdS/$CdSnO_3$ interface was invoked [46]. In situation like this, electron scavenging from CdS was counteracted to a certain extent, resulting in the prolonged fast decay component with diminished amplitude contribution (τ_2 = 0.30 ns, 88.4%). On the other hand, the electron–hole recombination across interface provided excited CdS with additional deactivation pathway which is essentially in long-lived state [15,47]. One would thus expect an extended time window for the excited state relaxation of CdS when $CdSnO_3$ with a relatively high content was present. This effect was confirmed by the slightly prolonged slow decay term as well as its enhanced contribution observed for CdS–$CdSnO_3$ with 5.0 at% $CdSnO_3$ (τ_1 = 4.84 ns, 11.6%). It might be argued that the surface states passivation by $CdSnO_3$ may contribute to the increase in emission lifetime of CdS. Because neither appreciable quantum yield recovery [46] nor apparent emission blue-shift [47] was noticed for CdS–$CdSnO_3$, the as-observed lifetime lengthening was not likely due to the passivation issue. To further certify this counteraction effect associated with interfacial electron–hole recombination, we collected and analyzed the carrier dynamics data for sample with even higher $CdSnO_3$ content. As can be seen in Table 1, when $CdSnO_3$ of 10.0 at% was present, the prolongation of slow and fast

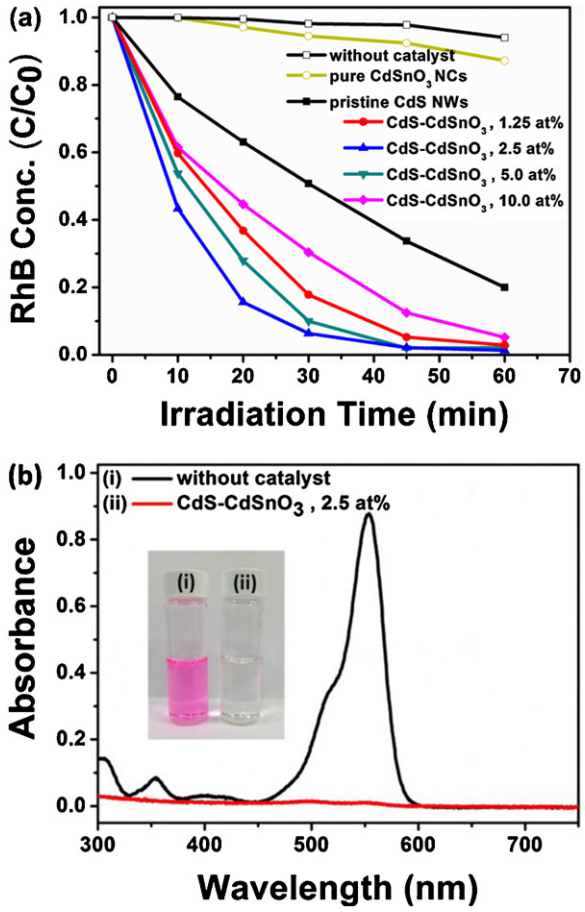

Fig. 4. (a) Results of RhB photodegradation for pristine CdS and CdS–$CdSnO_3$ NWs with different $CdSnO_3$ contents. (b) Absorption spectra of RhB solutions after exposure of 90 min of daytime sunlight without any sample and in the presence of CdS–$CdSnO_3$ NWs. Inset shows the corresponding solution color.

components and their variation in relative contribution became more noticeable (τ_1 = 6.48 ns with an enhanced contribution of 30.1% vs. τ_2 = 1.36 ns with a diminished contribution of 69.9%), suggesting that electron scavenging from CdS was counteracted by interfacial electron–hole recombination more significantly as 10.0 at% $CdSnO_3$ was introduced. This outcome demonstrates that excess $CdSnO_3$ may act as interfacial electron–hole recombination initiator which counteracted the degree of electron scavenging from CdS to suppress the overall charge separation efficiency.

To assess the quantitative effect of $CdSnO_3$ decoration on the photoconversion efficiency of CdS NWs, we performed photodegradation experiments by using RhB as the probe molecule. Note that RhB has an oxidation potential of +0.95 V vs. NHE making it a good hole acceptor for CdS–$CdSnO_3$ NWs [48]. When reacted with photogenerated holes, RhB undergoes one–hole oxidation to form $RhB^{\cdot+}$ which gets decomposed quickly via the de-alkylation process [49]. The decolorization of RhB under light illumination can thus be utilized to evaluate the photoconversion efficiency of the sample. Fig. 4(a) shows the photodegradation of RhB as a function of irradiation time over different samples. It is clearly seen that with the decoration of 1.25 at% $CdSnO_3$, CdS NWs performed better in RhB photodegradation. This improvement emanates from the deposited $CdSnO_3$ that can promote the carrier utilization efficiency of NWs by readily accepting photoexcited electrons from CdS, thereby leaving a considerable amount of photogenerated holes at CdS for participation in RhB degradation. For CdS–$CdSnO_3$ NWs with higher $CdSnO_3$ content (2.5 at%), an even better performance in RhB photodegradation was attained, mainly due to the much more efficient carrier utilization of NWs caused by the increasing amount of $CdSnO_3$. Nevertheless, a consecutively depressed performance of RhB photodegradation was observed as the content of $CdSnO_3$ was further increased to 5.0 and 10.0 at%. This phenomenon is consistent with those found in the literature, where the photocatalytic efficiency of type-II nanoheterostructures declines as the constituent content exceeds the optimal value [21–30]. Since $CdSnO_3$ itself did not effectively absorb visible light (absorption onset was around 400 nm) to hinder CdS from light absorption, the depressed photodegradation efficiency observed at 5.0 and 10.0 at% $CdSnO_3$ was not due to the inhibited light absorption issue [21–24]. Besides, no apparent aggregation of the grown $CdSnO_3$ was found in these samples, thus excluding the structural effect contention [21,25,26]. According to the deduction from carrier dynamics analysis, we considered that the emergence of electron–hole recombination across interface and its counteraction over electron scavenging were the main cause for the depressed photodegradation efficiency observed in the samples with 5.0 and 10.0 at% $CdSnO_3$. Because of the counteraction effect, the separated electrons at $CdSnO_3$ and the delocalized holes at CdS were significantly depleted. As a consequence of the less holes remaining at CdS, CdS–$CdSnO_3$ NWs with 5.0 and 10.0 at% $CdSnO_3$ showed depressed photocatalytic performance toward RhB degradation. Note that in the present case photogenerated holes were the exclusive oxidation species for RhB degradation, with which our arguments about the depleted holes at CdS for samples with 5.0 and 10.0 at% $CdSnO_3$ and the accordingly depressed RhB photodegradation can be validated. The direct hole-oxidation path for the current RhB photodegradation could be verified from the following comparative experiments. When tert-butyl alcohol, an effective ·OH radical scavenger [50], was added to RhB solution, no rate change of photodegradation was observed for CdS–$CdSnO_3$ NWs. On the other hand, if methanol, a typical hole scavenger [51], with a commensurate amount was introduced, pronounced suppression in RhB photodegradation resulted. Note that methanol has long been used as the hole acceptor for illuminated semiconductor particles [52,53]. The use of methanol in hole-scavenging experiment is thus essentially valid. These trials manifest that direct hole oxidation was the primary path for RhB photodegradation in the presence of CdS–$CdSnO_3$ NWs. It is important to state that all the CdS–$CdSnO_3$ samples show nearly identical RhB adsorption capability. After stirring in the dark for 30 min, CdS–$CdSnO_3$ NWs with 1.25, 2.5, 5.0, and 10.0 at% $CdSnO_3$ adsorbed 5.4, 2.6, 2.3, and 4.7% of RhB, respectively. This demonstration affirms that the variation in photodegradation efficiency for CdS–$CdSnO_3$ NWs with different $CdSnO_3$ contents is mainly related to the interfacial charge carrier dynamics rather than the structural effect associated with surface area or dye adsorption.

With the significant charge separation property and visible absorption capability, the present CdS–$CdSnO_3$ NWs may find promising potentials in solar energy harvesting and solar fuel generation, the two important features in photoconversion processes. This applicability can be explored by performing RhB photodegradation experiments under natural sunlight. As illustrated in Fig. 4(b), after exposure of 90 min of daytime sunlight, RhB was totally degraded by using CdS–$CdSnO_3$ NWs, accompanied by an obvious decolorization of the resultant solution. This outcome shows that CdS–$CdSnO_3$ NWs can effectively harvest energy from sunlight for practical photoconversion applications. To quantitatively compare the photoconversion efficiency of different samples, the apparent rate constant of RhB photodegradation (k_{RhB}) was calculated using the pseudo-first-order approximation. By use of the result of Fig. 4(a), we obtained k_{RhB} value of 0.025, 0.060, 0.081, 0.072, and 0.047 min^{-1} for pristine CdS and CdS–$CdSnO_3$ NWs with $CdSnO_3$ content of 1.25, 2.5, 5.0, and 10.0 at%, respectively. It is worth noting that the variation in RhB photodegradation rate of CdS–$CdSnO_3$ NWs with $CdSnO_3$ content corresponded well

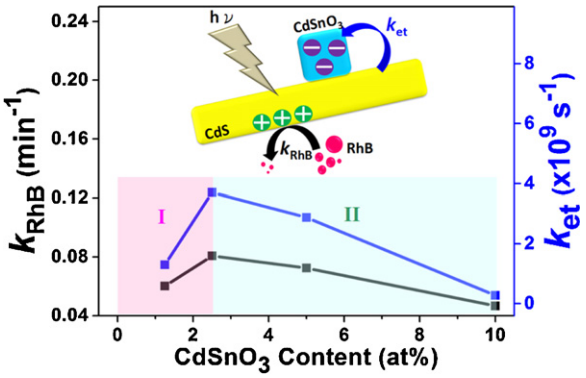

Fig. 5. Correlations of k_{et} and k_{RhB} with $CdSnO_3$ content for CdS–$CdSnO_3$ NWs.

with the result of carrier dynamics measurement. As depicted in Fig. 5, the correspondence can be realized by the competition between electron scavenging and interfacial electron–hole recombination at different $CdSnO_3$ content regions. Under a sufficiently low $CdSnO_3$ content condition (section I in Fig. 5), electron scavenging from CdS dominated the interfacial charge transfer of CdS–$CdSnO_3$, thus providing abundant charge carriers available for photodegradation utilization. In the situation of relatively high $CdSnO_3$ content (section II in Fig. 5), electron–hole recombination across CdS/$CdSnO_3$ interface was however prevalent, giving rise to a counteraction effect to deplete photoinduced charge carriers and thus the suppression in photoconversion efficiency. Based on the results obtained from the present investigation, we demonstrated that the counteraction effect associated with interfacial electron–hole recombination is the essentially important cause for the depressed photocatalytic efficiency of type-II semiconductor nanoheterostructures when the constituent content exceeds the optimal value.

4. Conclusions

In conclusion, the dependence of photoconversion efficiency on the constituent content for type-II semiconductor nanoheterostructures has been comprehended by analyzing the interfacial charge carrier dynamics of CdS–$CdSnO_3$ NWs. The carrier dynamics results are in good accordance with that of photoconversion performance evaluation in RhB photodegradation, demonstrating that the counteraction effect associated with electron–hole recombination across interface is the essentially important cause for the depressed photocatalytic efficiency of type-II nanoheterostructures when the constituent content exceeds the optimal value. The findings from this work may facilitate the use of type-II semiconductor nanoheterostructures in relevant photoconversion processes where the effectiveness of charge carrier separation is determinant.

Acknowledgment

This work was financially supported by the National Science Council of Republic of China (Taiwan) under grants NSC-100-2113-M-009-004 and NSC-101-3113-P-009-005.

References

[1] L. Wang, H. Wei, Y. Fan, X. Gu, J. Zhan, Journal of Physical Chemistry C 113 (2009) 14119–14125.
[2] A. Bera, D. Basak, ACS Applied Materials & Interfaces 2 (2010) 408–412.
[3] S. Cho, J.W. Jang, J. Kim, J.S. Lee, W. Choi, K.H. Lee, Langmuir 27 (2011) 10243–10250.
[4] T. Sasamura, K. Okazaki, A. Kudo, S. Kuwabata, T. Torimoto, RSC Advances 2 (2012) 552–559.
[5] S. Shenawi-Khalil, V. Uvarov, S. Fronton, I. Popov, Y. Sasson, Applied Catalysis B: Environmental 117–118 (2012) 148–155.
[6] Z. Zhang, W. Wang, L. Wang, S. Sun, ACS Applied Materials & Interfaces 4 (2012) 593–597.
[7] S. Shenawi-Khalil, V. Uvarov, S. Fronton, I. Popov, Y. Sasson, Journal of Physical Chemistry C 116 (2012) 11004–11012.
[8] L. Liu, J. Hensel, R.C. Fitzmorris, Y. Li, J.Z. Zhang, Journal of Physical Chemistry Letters 1 (2010) 155–160.
[9] W. Zhou, H. Liu, J. Wang, D. Liu, G. Du, J. Cui, ACS Applied Materials & Interfaces 2 (2010) 2385–2392.
[10] W. Zhu, X. Liu, H. Liu, D. Tong, J. Yang, J. Peng, Journal of the American Chemical Society 132 (2010) 12619–12626.
[11] G. Wang, X. Yang, F. Qian, J.Z. Zhang, Y. Li, Nano Letters 10 (2010) 1088–1092.
[12] J. Hensel, G. Wang, Y. Li, J.Z. Zhang, Nano Letters 10 (2010) 478–483.
[13] Y. Shemesh, J.E. Macdonald, G. Menagen, U. Banin, Angewandte Chemie International Edition 50 (2011) 1185–1189.
[14] A. Salant, M. Shalom, Z. Tachan, S. Buhbut, A. Zaban, U. Banin, Nano Letters 12 (2012) 2095–2100.
[15] K. Das, S.K. De, Journal of Physical Chemistry C 113 (2009) 3494–3501.
[16] S.S. Lo, T. Mirkovic, C.H. Chuang, C. Burda, G.D. Scholes, Advanced Materials 23 (2011) 180–197.
[17] Y.-C. Chen, Y.-C. Pu, Y.-H. Hsu, Journal of Physical Chemistry C 116 (2012) 2967–2975.
[18] A. Kongkanand, K. Tvrdy, K. Takechi, M. Kuno, P.V. Kamat, Journal of the American Chemical Society 130 (2008) 4007–4015.
[19] V. Chakrapani, K. Tvrdy, P.V. Kamat, Journal of the American Chemical Society 132 (2010) 1228–1229.
[20] K. Tvrdy, P.A. Frantsuzovc, P.V. Kamat, Proceedings of the National Academy of Sciences 108 (2011) 29–34.
[21] L. Huang, F. Peng, H. Wang, H. Yu, Z. Li, Catalysis Communications 10 (2009) 1839–1843.
[22] M. Niu, F. Huang, L. Cui, P. Huang, Y. Yu, Y. Wang, ACS Nano 4 (2010) 681–688.
[23] S. Wei, Y. Ma, Y. Chen, L. Liu, Y. Liu, Z. Shao, Journal of Hazardous Materials 194 (2011) 243–249.
[24] D. He, L. Wang, D. Xu, J. Zhai, D. Wang, T. Xie, ACS Applied Materials & Interfaces 3 (2011) 3167–3171.
[25] A.I. Kontos, V. Likodimos, T. Stergiopoulos, D.S. Tsouk-leris, P. Falaras, I. Rabias, G. Papavassiliou, D. Kim, J. Kunze, P. Schmuki, Chemistry of Materials 21 (2009) 662–672.
[26] Y.C. Zhang, Z.N. Du, K.W. Li, M. Zhang, D.D. Dionysiou, ACS Applied Materials & Interfaces 3 (2011) 1528–1537.
[27] H. Cheng, B. Huang, Y. Dai, X. Qin, X. Zhan, Langmuir 26 (2010) 6618–6624.
[28] I. Paramasivam, Y.C. Nah, C. Das, N.K. Shrestha, P. Schmuki, Chemistry: A European Journal 16 (2010) 8993–8997.
[29] Z. Wang, B. Huang, Y. Dai, X. Qin, X. Zhang, P. Wang, H. Liu, J. Yu, Journal of Physical Chemistry C 113 (2009) 4612–4617.
[30] C. Xu, L. Cao, G. Su, W. Liu, H. Liu, Y. Yu, X. Qu, Journal of Hazardous Materials 176 (2010) 807–813.
[31] Y. Xu, M.A.A. Schoonen, American Mineralogist 85 (2000) 543–556.
[32] G. Natu, Y. Wu, Journal of Physical Chemistry C 114 (2010) 6802–6808.
[33] Y.-J. Hsu, S.-Y. Lu, Small 4 (2008) 951–955.
[34] Y.-J. Hsu, S.-Y. Lu, Y.-F. Lin, Chemistry of Materials 20 (2008) 2854–2856.
[35] S. Sadhu, M. Tachiya, A. Patra, Journal of Physical Chemistry C 113 (2009) 19488–19492.
[36] M. Li, S.K. Cushing, Q. Wang, X. Shi, L.A. Hornak, Z. Hong, N. Wu, Journal of Physical Chemistry Letters 2 (2011) 2125–2129.
[37] W.S. Chae, J.H. Ko, I.W. Hwang, Y.R. Kim, Chemical Physics Letters 365 (2002) 49–56.
[38] S. Sadhu, P.S. Chowdhury, A. Patra, Journal of Luminescence 128 (2008) 1235–1240.
[39] I.V. Lightcap, P.V. Kamat, Journal of the American Chemical Society 134 (2012) 7109–7116.
[40] C. Harris, P.V. Kamat, ACS Nano 3 (2009) 682–690.
[41] C. Harris, P.V. Kamat, ACS Nano 4 (2010) 7321–7330.
[42] X. Zhang, L. Zhang, T. Xie, D. Wang, Journal of Physical Chemistry C 113 (2009) 7371–7378.
[43] H. Zhang, R. Zong, Y. Zhu, Journal of Physical Chemistry C 113 (2009) 4605–4611.
[44] Y.-C. Pu, Y.-C. Chen, Y.-J. Hsu, Applied Catalysis B: Environmental 97 (2010) 389–397.
[45] X. Liu, L. Pan, T. Lv, G. Zhu, Z. Sun, C. Sun, Chemical Communications 47 (2011) 11984–11986.
[46] C.H. Chuang, S.S. Lo, G.D. Scholes, C. Burda, Journal of Physical Chemistry Letters 1 (2010) 2530–2535.
[47] S. Rawalekar, S. Kaniyankandy, S. Verma, H.N. Ghosh, Journal of Physical Chemistry C 114 (2010) 1460–1466.
[48] Z. Xiong, L.L. Zhang, J. Ma, X.S. Zhao, Chemical Communications 46 (2010) 6099–6101.
[49] T. Takirawa, T. Watanabe, K. Honda, Journal of Physical Chemistry 82 (1978) 1391–1396.
[50] S.C. Yan, Z.S. Li, Z.G. Zou, Langmuir 26 (2010) 3894–3901.
[51] J. Zhuang, W. Dai, Q. Tian, Z. Li, L. Xie, J. Wang, P. Liu, Langmuir 26 (2010) 9686–9694.
[52] R.F. Howe, M. Gratzel, Journal of Physical Chemistry 89 (1985) 4495–4499.
[53] L. Spanhel, H. Weller, A. Henglein, Journal of the American Chemical Society 109 (1987) 6632–6635.